Speckle noise reduction in OCT and projection images using hybrid wavelet thresholding

X. Sui[1], H. Ishikawa[2], I. W. Selesnick[1], G. Wollstein[2], J. S. Schuman[2]

1. NYU Tandon School of Engineering, New York, NY, USA

2. NYU Langone Eye Center, NYU School of Medicine, New York, NY, USA

{xs405, iws211}@nyu.edu, {Hiroshi.Ishikawa, Gadi.Wollstein}@nyumc.org, Joel.Schuman@med.nyu.edu

Abstract—Speckle noise in optical coherence tomography (OCT) images is a granular noise that inherently exists and degrades the image quality. The challenge of conventional denoising methods is to distinguish the informational pattern from the speckle noise. In this paper we present a novel method for speckle noise reduction in OCT volumes, where the corresponding en face representation, which produces frontal sections of retinal layers and is relatively free of speckle, is considered as a reference. The proposed method estimates the anatomical structures by solving a constrained optimization problem that combines wavelet-domain sparsity and total variation (wavelet-TV) regularization to preserve the edges of retinal layers and to alleviate artifacts introduced by pure wavelet thresholding. Denoising performance is evaluated through the signal to noise ratio (SNR) and the contrast to noise ratio (CNR). The volumes processed by the proposed method show notable reduction of speckle without losing details in both en face and cross-sectional images.

I. Introduction

Optical Coherence Tomography (OCT) is an in vivo and non-invasive imaging technique that has been widely used [1]. OCT is based on low-coherence interferometry, which relies inherently on the spatial and temporal coherence of the optical waves backscattered from observed sample [2]. But this coherence also gives rise to speckle [2]. Speckle noise degrades the image quality of OCT tomograms by reducing contrast and obscuring boundaries, and has a negative effect on subsequent image analysis, such as image segmentation and pattern recognition.

Besides the direct representation of a large 3D volume or numerous 2D cross-sectional images, an en face representation of OCT has also been used, especially for detecting retinal abnormalities and registering with color fundus photography. The en face fundus image, also known as projection OCT fundus imaging, is generated by summing the retinal layers along the depth axis [3], as illustrated in Fig 1. This procedure reduces the effects of noise and enhances image quality [3].

One of the main difficulties in developing successful speckle noise reduction algorithms is to separate noise and information of observed sample in a speckle pattern. One type of existing method is to reduce speckle during data acquisition procedure. For example, the compounding techniques, which average multiple uncorrelated recordings [4], are widely used. This class of methods is not preferred because it is time consuming and requires additional imaging system hardware modification. Therefore, noise reduction methods based on image processing techniques are more favorable. A number of speckle reduction algorithms such
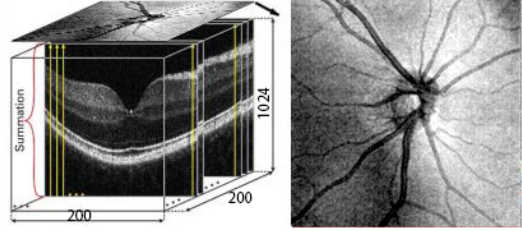

Figure 1: A typical retinal OCT volume and en face (projection OCT fundus) image

as locally adaptive filtering [5], soft thresholding of the wavelet sub-bands [6], and neural networks [7] have been proposed.

In this paper we propose a novel speckle noise reduction algorithm via solving a convex optimization problem. The objective function to be minimized is defined based on the assumption that the underlying OCT data is a sum of two components: (i) the clean structures, which are smooth patterns with sharp edges and (ii) the spatially sparse speckle noise. In the proposed approach, the two components are decomposed and penalized by a unified wavelet-TV regularization and l_1 norm, respectively. Moreover, the en face fundus information is also considered as a constraint in this optimization problem. The proposed method is computationally efficient and converges fast.

The rest of this paper is organized as follows. We list the preliminaries in Section II and the speckle removal model in Section III. We illustrate the efficiency of proposed method with various examples in Section IV. Conclusions follow in Section V.

II. Preliminaries

A. Notation

The volume signal with the size of $N_1 \times ... \times N_D$ is represented by a D-mode tensor $x \in \mathbb{R}^{N_1 \times ... \times N_D}$ with entries $x_{i_1...i_D}$ where $1 \leq i_j \leq N_j$ for $1 \leq j \leq D$. The mode-j one-dimensional fiber $x^{[j]} = x_{i_1,..i_{j-1},:,i_{j+1},...,i_D} \in \mathbb{R}^{N_j}$ is the high order analogue of matrix rows and columns. For simplicity of notation, we use $/\{i_j\}$ to represent the index set excluding i_j, i.e., $\{i_1, ..., i_{j-1}, i_{j+1}, ..., i_D\}$. The l_2-norm of x is defined as

$$\|x\|_2 = \left(\sum_{i_1,i_2,...,i_D} |x_{i_1,i_2,...,i_D}|^2 \right)^{\frac{1}{2}}. \qquad (1)$$

The projection function P_j is defined as axially summation along dimension j, which is,

$$P_j(x) = \sum_{i_j=0}^{N_j-1} x_{i_1 i_2 \ldots, i_j, \ldots i_D}, \qquad (2)$$

The soft-threshold function [9] for $\lambda > 0$ is defined as

$$\text{soft}(x, \lambda) = \begin{cases} x - \lambda \, \text{sign} \, x, & |x| > \lambda \\ 0, & |x| \leq \lambda \end{cases} \qquad (3)$$

B. Multidimensional total variation

Denote $\text{TV}_j(x)$ as the differential operator along the j-th dimension of x with the form of

$$\text{TV}_j(x) = \sum_{/\{i_j\}} \sum_{i_j=1}^{N_j-1} |x_{i_1, \ldots i_j, \ldots i_D} - x_{i_1, \ldots (i_j+1), \ldots i_D}|. \quad (4)$$

The weighted l_1 norm based anisotropic TV regularizer can be defined as

$$\text{TV}(x, \beta) = \sum_{j=1}^{D} \beta_j \, \text{TV}_j(x), \qquad (5)$$

where $\beta_j, j = 1, ..., D$ are nonnegative regularizer parameters.

C. Wavelet transform

The wavelet transform, which reorganizes image into a low-resolution approximation and a set of details, is employed since it compresses the essential information into a few large coefficients, whereas noise tends to be spread insignificantly [10]. Simple thresholding of wavelet coefficients is an efficient way to restore signals that admit a sparse wavelet representation from its noisy version [11].

We denote the wavelet transform as W and the wavelet coefficients of signal x as $w_{j,\Omega} = W(x)$ where j and Ω are the scale and space indices, respectively. We assume that W is a tight frame, i.e.,

$$W^* \circ W = \text{Id}. \qquad (6)$$

In this work, the 3D dual-tree complex wavelet transform ($\mathbb{C}$WT) is used. The proposed algorithm can be used with any tight frame satisfying (6).

III. SPECKLE REMOVAL MODEL

A. Problem formulation

We model the observed OCT signal y as

$$y = x + s + w, \qquad (7)$$

where x represents the noise-free OCT data, s consists of speckles, and w is the additive white Gaussian noise. The estimate of the components x and s from the noisy observation y is expressed as the following optimization problem:

$$\arg \min_{x,s} \left\{ G(x) = \frac{1}{2} \|y - x - s\|_2^2 + \rho \|s\|_1 \right.$$
$$\left. + \sum_{j,\Omega} \lambda_j |[W(x)]_{j,\Omega}| + \text{TV}(x, \beta) + \frac{\gamma}{2} \|P_d(x) - P_d(y)\|_2^2 \right\}.$$
$$(8)$$

where the projection $P_d(\cdot)$, which is given in (2), represents summation along the depth axis d of a OCT volume. $W(\cdot)$ indicates the wavelet transform and $\text{TV}(\cdot)$ represents the TV regularization defined in (5). The scalars $\rho > 0$, $\lambda_j > 0$, $\gamma > 0$ and the vector $\beta > 0$ are regularization parameters. We set the wavelet regularization λ_j vary with scale j. γ controls the similarity between the projection of clean image and observed raw image. In this algorithm, the parameters could be set manually or based on the observed image.

B. Algorithm

The objective function in (8) is strictly convex, and can be minimized via convex optimization algorithms. To solve the problem (8), we use the the well-known alternating direction method of multipliers (ADMM) [12], which is a special case of powerful proximal method (Douglas-Rachford splitting) [13] [14]. Applying variable splitting, we rewrite (8) as

$$\arg \min_{x,v,s,u} \left\{ \frac{1}{2} \|y - x - s\|_2^2 + \rho \|u\|_1 + \sum_{i=0}^{D} g_i(v_i) + h(v_{D+1}) \right\}$$
$$\text{s.t.,} \quad x = v_i, \quad i = 0, ..., K$$
$$s = u$$
$$(9)$$

where $K = D + 1$ and

$$g_0(v_0) = \sum_{j,\Omega} \lambda_j |[W(v_0)]_{j,\Omega}|,$$
$$g_i(v_i) = \beta_i \, \text{TV}_i(v_i), \quad i = 1, ..., D \qquad (10)$$
$$h(v_K) = \frac{\gamma}{2} \|P_d(v_K) - P_d(y)\|_2^2.$$

Solving (9) is equivalent to iteratively minimize the scaled augmented Lagrangian [12] with respect to (x, s) and (v_i, u) alternately, as proven in [14]. Thereby, in each iteration we carry out the following steps:

$$(x, s) = \arg \min_{x,s} \left\{ \frac{1}{2} \|y - x - s\|_2^2 + \frac{\mu}{2} \Big[\|s + d_s - u\|_2^2 \right.$$
$$\left. + \sum_{i=0}^{K} \|x + d_i - v_i\|_2^2 \Big] \right\} \qquad (11a)$$

$$(v, u) = \arg \min_{v,u} \left\{ \rho \|u\|_1 + \sum_{i=0}^{D} g_i(v_i) + h(v_K) \right.$$
$$\left. + \frac{\mu}{2} \Big[\|s + d_s - u\|_2^2 + \sum_{i=0}^{K} \|x + d_i - v_i\|_2^2 \Big] \right\} \qquad (11b)$$

$$d_i = d_i + (x - v_i) \quad i = 0, ..., K \qquad (11c)$$
$$d_s = d_s + (s - u). \qquad (11d)$$

Step 1: solving the sub-problem for (x, s). To derive the solution to (11a), we define the following substitutions

$$\mathbf{x} = \begin{bmatrix} x \\ s \end{bmatrix}, \mathbf{v} = \begin{bmatrix} v_0 \\ \vdots \\ v_{D+1} \\ u \end{bmatrix}, \mathbf{d} = \begin{bmatrix} d_0 \\ \vdots \\ d_{D+1} \\ d_s \end{bmatrix}, \mathbf{G} = \begin{bmatrix} I & 0 \\ \vdots & \vdots \\ I & 0 \\ 0 & I \end{bmatrix}$$
$$(12)$$

and $\mathbf{M} = [\mathbf{I}, \mathbf{I}]$. We rewrite (11a) as

$$\mathbf{x} = \arg\min_{\mathbf{x}} \left\{ \frac{1}{2}\|\mathbf{y} - \mathbf{Mx}\|_2^2 + \frac{\mu}{2}\|\mathbf{Gx} + \mathbf{d} - \mathbf{v}\|_2^2 \right\}. \tag{13}$$

The exact and explicit solution to (13) can be found by solving the following linear equations

$$(\mathbf{M}^\mathsf{T}\mathbf{M} + \mu\mathbf{G}^\mathsf{T}\mathbf{G})\mathbf{x} = \mathbf{M}^\mathsf{T}\mathbf{y} + \mu\mathbf{G}^\mathsf{T}(\mathbf{v} - \mathbf{d}), \tag{14}$$

which are equivalent to

$$\begin{cases} (1 + \mu(D + 2))x + s = y + \mu\sum_{i=0}^{K}(v_i - d_i) \\ x + (1 + \mu)s = y + \mu(u - d_s). \end{cases} \tag{15}$$

Step 2: solving the sub-problem for (v, u). The minimization in (11b) is separable, thus the optimal v and u can be found independently. Then we can rewrite (11b) as

$$u = \arg\min_{u} \left\{ \frac{\mu}{2}\|s + d_s - u\|_2^2 + \rho\|u\|_1 \right\} \tag{16a}$$

$$v_0 = \arg\min_{v_0} \left\{ \frac{\mu}{2}\|x + d_0 - v_0\|_2^2 \right.$$
$$\left. + \sum_{j,\Omega} \lambda_j |[W(v_0)]_{j,\Omega}| \right\} \tag{16b}$$

$$v_i = \arg\min_{v_i} \left\{ \frac{\mu}{2}\|x + d_i - v_i\|_2^2 + \beta_i\,\mathrm{TV}_i(v_i) \right\} \tag{16c}$$

$$v_K = \arg\min_{v_K} \left\{ \frac{\mu}{2}\|x + d_K - v_K\|_2^2 \right.$$
$$\left. + \frac{\gamma}{2}\|P_d(v_K) - P_d(y)\|_2^2 \right\}. \tag{16d}$$

Solution to (16a) is implemented using the soft thresholding function as

$$u = \mathrm{soft}(s + d_s, \rho/\mu). \tag{17}$$

Problem (16b) can also be solved exactly. Define

$$Q(z_0) = \arg\min_{v_0} \left\{ \frac{1}{2}\|z_0 - v_0\|_2^2 + \psi(W(v_0)) \right\} \tag{18a}$$

$$= \mathrm{prox}_{\psi \circ W}(z_0) \tag{18b}$$

$$= (\mathrm{Id} + W^* \circ (\mathrm{prox}_\psi - \mathrm{Id}) \circ W)(z_0), \tag{18c}$$

where $z_0 = x + d_0$ and $\psi(\cdot) = \sum_{j,\Omega} \lambda_j/\mu |[\cdot]_{j,\Omega}|$. To derive (18c) from (18b), we use the semi-orthogonal linear transform property of proximal operator [13]. The proximal operator of ψ is defined by

$$\mathrm{prox}_\psi(q) = \arg\min_{p} \left\{ \frac{1}{2}\|q - p\|_2^2 + \sum_{j,\Omega} \frac{\lambda_j}{\mu}|p_{j,\Omega}| \right\} \tag{19}$$

Since the problem (19) is separable, it can be written as

$$[\mathrm{prox}_\psi(q)]_{j,\Omega} = \arg\min_{p} \left\{ \frac{1}{2}(q_{j,\Omega} - p_{j,\Omega})^2 + \frac{\lambda_j}{\mu}|p_{j,\Omega}| \right\}$$
$$= \mathrm{soft}(q_{j,\Omega}, \lambda_j/\mu), \tag{20}$$

which is an element-wise thresholding function. The sub-problem (16c) is separable. For simplicity, we use s, t to represent the corresponding mode-i fiber of v_i and $z_i =$

$x + d_i$, i.e., $s = (v_i)^{[i]}$ and $t = (z_i)^{[i]}$. Then (16c) can be decomposed into a set of independent TV problems

$$s = \arg\min_{s} \left\{ \frac{1}{2}\|t - s\|^2 + \frac{\beta_i}{\mu}\sum_{j=1}^{N_i - 1}|s_j - s_{j+1}| \right\} \tag{21}$$

for all $j_1, ..., j_{i-1}, j_{i+1}, ...j_d$ and they can be solved efficiently by a fast finite-time algorithm [15]. Finally, v_K can be updated by solving a least square problem (16d). We rewrite the tensor v as a vector $\mathbf{v}$ by rearranging the dimensions of v in the order specified by index set $\{i_d, i_1, ..., i_{d-1}, j_{d+1}, ..., i_D\}$. Then the projection (2) can be rewritten as $P_d(v) = \mathbf{Sv}$ with the following substitution.

$$\mathbf{S} = \begin{bmatrix} \overbrace{1 \quad \cdots \quad 1}^{N_d} & & & \\ & \overbrace{1 \quad \cdots \quad 1}^{N_d} & & \\ & & \ddots & \\ & & & \underbrace{1 \quad \cdots \quad 1}_{N_d} \end{bmatrix} \left.\rule{0pt}{40pt}\right\} \prod_{\Sigma / \{i_j\}} \tag{22}$$

In this way, solution to (16d) can be written as

$$v_K = (\mathbf{I} + \gamma/\mu\mathbf{S}^\mathsf{T}\mathbf{S})^{-1}(z_K + \gamma/\mu\mathbf{S}^\mathsf{T}\mathbf{S}y), \tag{23}$$

where $z_K = x + d_K$. Using the matrix inverse lemma, we write

$$(\mathbf{I} + \gamma/\mu\mathbf{S}^\mathsf{T}\mathbf{S})^{-1} = \mathbf{I} - \mathbf{S}^\mathsf{T}\left(\mu/\gamma\mathbf{I} + \mathbf{SS}^\mathsf{T}\right)^{-1}\mathbf{S}$$
$$= \mathbf{I} - \gamma/(\mu + \gamma N_d)\mathbf{S}^\mathsf{T}\mathbf{S}, \tag{24}$$

where the matrix $\mathbf{SS}^\mathsf{T} = N_d\mathbf{I}$ is diagonal. Thus, updating v_K only consists of simple addition and multiplication, rather than finding matrix inverse or solving system of linear equations.

Step 3: updating d. In each iteration, $d_i, i = 0, ..., K$ and d_s are updated using (11c) and (11d), respectively. Combining the routines discussed above, we obtain the following algorithm.

C. Parameters setting

We also suggest an automatic way to set required parameters in proposed algorithm. First, we set $D = 3$ so that we reduce speckle in 3D scans directly. Second we consider to set parameters λ_i and β in pair. There are two special cases that could provide anchors for the selection of λ_i and β. In the first case, $\lambda_i = 0$ and problem (8) trends to be a pure wavelet denoising problem with parameter λ^*. In the second case, $\beta = 0$ so problem (8) reduces to be a TV problem with the suitable parameters β^*. In this work, we set

$$\lambda = \eta\lambda^*, \quad \beta = (1 - \eta)\beta^*, \tag{25}$$

where $0 < \eta < 1$ controls a trade-off between wavelet thresholding and TV regularization. Here we suggest setting $\eta = 0.9$ so that TV regularization only works as a minor adjustment in order to not only reduce artifacts introduced by pure wavelet thresholding but also avoid artificial discontinuity appearance.

Algorithm 1 OCT Denoising Algorithm

1: **Inputs:**
$\quad\quad y, \rho, \lambda_j, \beta, \mu$
2: **Initialize:**
$\quad\quad v_s = 0, d_s = 0, v_i = 0, d_i = 0$
3: **repeat**
4: $\quad\quad A = y + \mu \sum_{i=0}^{D+1}(v_i - d_i)$
5: $\quad\quad B = y + \mu(u - d_s)$
6: $\quad\quad C = (1+D)\mu^2 + (2+D)\mu$
7: $\quad\quad x = ((1+\mu)A - B)/C$
8: $\quad\quad s = ((1 + (2+D)\mu)B - A)/C$
9: $\quad\quad z_0 = x + d_0$
10: $\quad\quad p_{j,\Omega} = \text{soft}([W(z_0)]_{j,\Omega}, \lambda_j/\mu), \quad \forall j, \Omega$
11: $\quad\quad v_0 = z_0 + W^*(p - W(z_0))$
12: $\quad\quad v_i = \text{tvd}(x + d_i, \beta_i/\mu), \quad i = 1, ..., D$
13: $\quad\quad q = x + d_{D+1} + \gamma/\mu \mathbf{S}^{\mathsf{T}}\mathbf{S}y$
14: $\quad\quad v_{D+1} = q - \gamma/(\mu + \gamma N_d)\mathbf{S}^{\mathsf{T}}\mathbf{S}q$
15: $\quad\quad u = \text{soft}(s + d_s, \rho/\mu)$
16: $\quad\quad d_i = d_i + x - v_i, \quad i = 0, ..., D+1$
17: $\quad\quad d_s = d_s + s - u$
18: **until** convergence
19: **Outputs:**
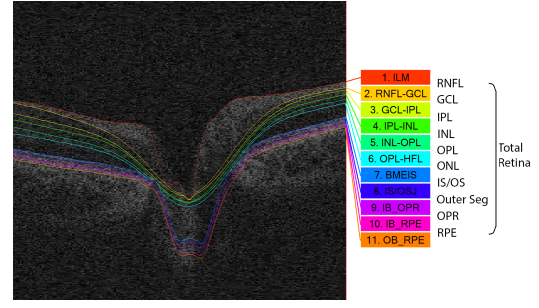$\quad\quad x, s$

Figure 2: Illustration of layers segmented using Iowa Reference Algorithm. (left) One example frame with segmentations. Colored labels indicate the name of 11 surfaces (middle) and 10 layers (right).

There are some discussions about setting regularization parameters in a signal restoration problem [16]. Here we use a similar approach to set λ^* and β^*. We seek to set λ^* so that the optimal solution to the wavelet denoising problem is relatively noise-free with high probability. We set the wavelet thresholds $\lambda_i^* = C_\lambda \sigma_i$, where σ_i denotes the noise standard deviation in wavelet scale i. For the dual-tree wavelet transform discussed in section II-C, σ_i in each scale i are the same and equal to the noise standard deviation σ in the signal domain. For the TV denoising problem, $\beta_j^* = C_\beta \sqrt{N_j}\sigma$ is used in 1D case as discussed in [17]. Therefore we set

$$\lambda_i = \eta\sigma, \quad \beta_j = (1 - \eta)\sqrt{N_j}\sigma, \quad (26)$$

where N_j for $j = 1, 2, 3$ are the length of volume in each dimension j. In this work, we estimate σ using a gaussian mixture model (GMM) based on the empirical statistical analysis of OCT images. A 2-component GMM is a good estimation of the histogram of OCT images. The component with smaller mean value represents the background speckle very well. Therefore, we set the standard deviation of the first gaussian model to be σ.

The choices of regularization parameters ρ and γ are highly related to the noise level σ of raw images as well. Intuitively, we set

$$\rho = C_\rho \sigma, \quad \gamma = C_\gamma \sigma / N_d, \quad (27)$$

where N_d is the length of volume along the projection dimension d. In this work, we suggest setting $C_1 = 1$ and $C_2 = 0.5$.

IV. EXPERIMENTAL RESULTS

A. Quantitative evaluation metrics

The performance is evaluated in a quantitative way using peak signal to noise ratio (SNR) and contrast to noise ratio (CNR). They are presented below:

$$\text{SNR} = 10 \log_{10}\left[\frac{\max(I^2)}{\sigma_b^2}\right], \quad (28)$$

$$\text{CNR} = \frac{1}{R}\left[\sum_{r=1}^{R}\frac{\mu_r - \mu_b}{\sqrt{\sigma_r^2 + \sigma_b^2}}\right], \quad (29)$$

where μ_b and σ_b^2 represent the mean and variance of the background noise region, and I represents image intensity. μ_r and σ_r^2 represents the mean and variance of the r-th region of interest (ROI). R is the total number of regions used for the algorithm evaluation.

In this paper, the evaluation procedure is described as follows. First of all, 11 retinal surfaces (10 layers) are segmented using Iowa Reference Algorithm [18]. Then the region above nerve fiber layer (RNFL) is selected as the background, in which only noise is contained. The boundary between the background and RNFL is the internal limiting membrane (ILM) surface (the red line in Fig. 2). And all the 10 layers, including NFL, ganglion cell layer (GCL), inner plexiform layer (IPL), inner nuclear layer (INL), outer plexiform layer (OPL), outer nuclear layer (ONL), junction of inner and outer photoreceptor segments (IS/OS), outer segment (OS), outer segment PR/RPE complex (OPR) and retinal pigment epithelium complex (RPE+) [19], are selected as the 10 regions of interest. Fig. 2 illustrates a 10-layer segmentation for sample OCT images. The 10 regions are marked for evaluation. Finally, SNR and CNR are calculated for every ROI. Each of the volumes has 10 SNR and 10 CNR numbers, respectively. Further statistic analysis (like mean, variance) of evaluation metrics numbers are applied for performance comparison between different denoising algorithms.

B. Data from normal subject eyes

In this paper, we first test the algorithm using 3D OCT volumes captured from 12 out of 37 healthy volunteers.

(a) Raw image   (b) Proposed method

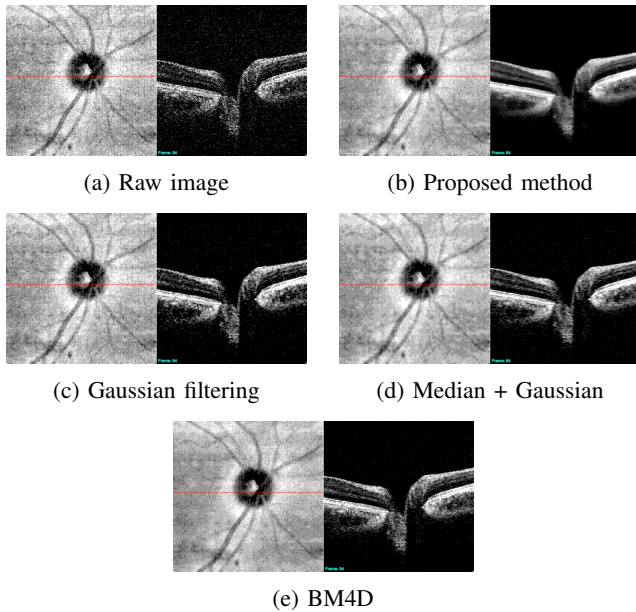(c) Gaussian filtering   (d) Median + Gaussian

(e) BM4D

Figure 3: Sample OCT en face and cross-sectional images (original images (a) with SS=4). Proposed method (b) notably reduces the speckle noise without losing details. Gaussian (c) and mixed filters (d) blurs borders of retinal layers, while BM4D (e) preserves edges.

(a) Proposed, denoising level 1   (b) BM4D, denoising level 1

(c) Proposed, denoising level 2   (d) BM4D, denoising level 2

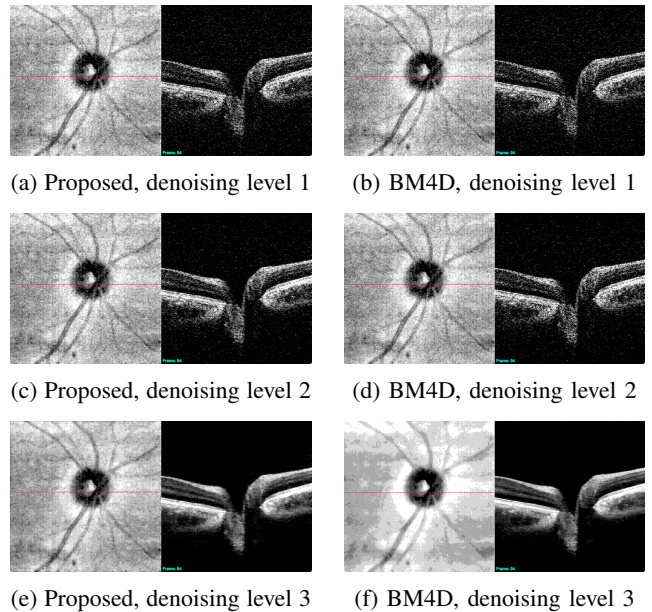(e) Proposed, denoising level 3   (f) BM4D, denoising level 3

Figure 4: A comparison between proposed method (4a)(4c)(4e) and BM4D (4b)(4d)(4f) with different denoising levels. BM4D blurs the en face image compared to proposed method under same denoising level.

The volunteers were scanned with Cirrus HD-OCT (Zeiss, Dublin, CA) device 10 times on the same day. During the scanning, the signal strength (SS) of the scanned images were controlled by adding different testing lens in between the subject eye and the OCT scanner. So for each subject eye, 10 scanned images with the signal strength varied from 1 to 10 were captured.

To compare with other methods, BM4D [20], which is a patch-based transform-domain filtering method and the current standard for denoising medical images, as well as two conventional spatial domain filtering methods, including three-dimensional Gaussian filtering and mixed median (on z axis) and Gaussian (on cross-sectional images) filtering are used.

A visual comparison of sample en face and cross-sectional images before and after processing are presented in Fig. 3. The signal strength of all the samples is 4. In this challenging low signal quality situation, the proposed method provides noticeably improved speckle noise suppression without losing details in both en face and cross-sectional images. Both BM4D and proposed method preserve edges well, but some residual speckle pattern is still visible in the background after processing by BM4D. Gaussian and mixed filters result in limited noise reduction and these two methods also blur borders of retinal layers. In addition, the proposed method makes the texture of retinal layers more homogeneous which may improve segmentation quality.

A further comparison between the proposed method and BM4D is illustrated in Fig. 4. We manually tune the parameters in both algorithms in order to achieve a similar noise reduction level. Both methods deliver improved noise suppression and make retina layers more homogeneous when the denoising level is higher. But BM4D over smooths the appearance of morphological features in en face images (vessels in the bottom right corner of Fig. 4f) compared to the proposed method under similar noise reduction level.

Fig. 5 demonstrates a comparison of image quality metrics. We observe that the proposed method achieves higher mean SNR and CNR than all the other methods under all signal strength. Moreover, the proposed method outperforms reference methods in terms of SNR more significantly when signal quality is low (SS $\leq$ 4).

C. Data from other collaborators

The algorithm is also tested on another individual dataset provided by collaborators in Korea, in order to show the generalization ability of proposed algorithm. The OCT volumes were acquired using similar device (Cirrus HD-OCT) and settings. The signal strength was fixed to be high enough to acquire acceptable image quality. We process 25 volumes in a similar way described in section IV-B and also calculate SNR and CNR as evaluation metrics. Seen from Fig. 6, the proposed denoising method shows statistically significantly higher SNR and CNR than all the other conventional filters.

V. CONCLUSION

This paper describes a OCT model comprising of (i) informational patterns, which are penalized by wavelet-TV regularization, and (ii) speckle which has spatial sparse appearance. Projection OCT fundus images are also
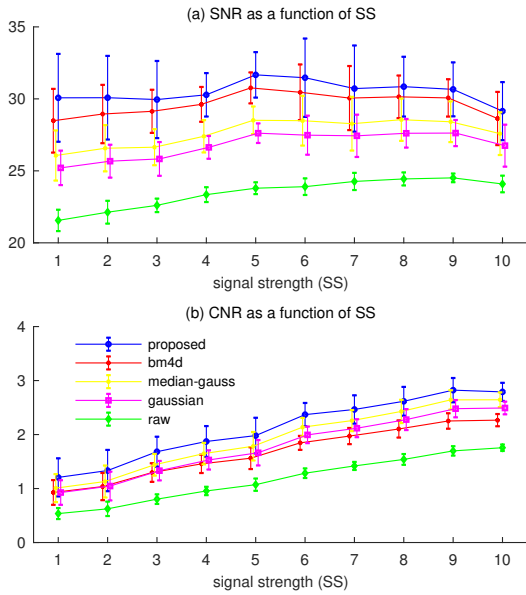
Figure 5: Statistical analysis of SNR (a) and CNR (b) as a function of SS
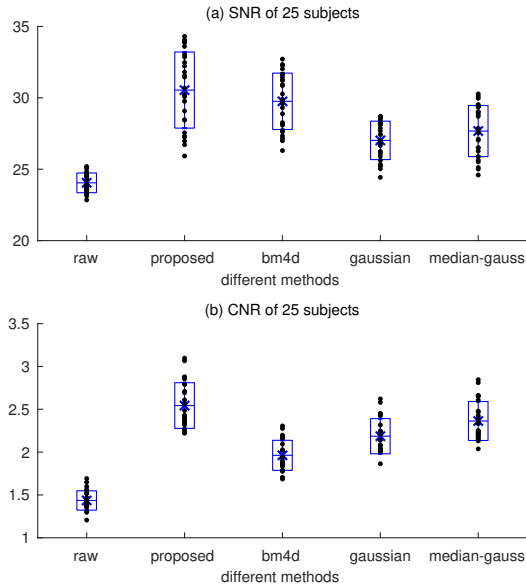

Figure 6: Statistical analysis of SNR (a) and CNR (b) on 25 patients

introduced in the model to avoid over-smoothing. We propose a convex optimization based algorithm for speckle noise reduction, which estimates the two components in the signal model. This method, tested on experimental examples, outperforms conventional methods in SNR and CNR.

REFERENCES

[1] D. Huang, E. A. Swanson, C. P. Lin, J. S. Schuman, W. G. Stinson, W. Chang, M. R. Hee, T. Flotte, K. Gregory, C. A. Puliafito *et al.*, "Optical coherence tomography," *Science*, vol. 254, no. 5035, pp. 1178–1181, 1991.

[2] J. M. Schmitt, S. Xiang, and K. M. Yung, "Speckle in optical coherence tomography," *Journal of Biomedical Optics*, vol. 4, no. 1, pp. 95–106, 1999.

[3] I. Gorczynska, V. J. Srinivasan, L. N. Vuong, R. W. Chen, J. J. Liu, E. Reichel, M. Wojtkowski, J. S. Schuman, J. S. Duker, and J. G. Fujimoto, "Projection oct fundus imaging for visualising outer retinal pathology in non-exudative age-related macular degeneration," *British Journal of Ophthalmology*, vol. 93, no. 5, pp. 603–609, 2009.

[4] A. Desjardins, B. Vakoc, W. Oh, S. Motaghiannezam, G. Tearney, and B. Bouma, "Angle-resolved optical coherence tomography with sequential angular selectivity for speckle reduction," *Optics Express*, vol. 15, no. 10, pp. 6200–6209, 2007.

[5] J. Rogowska and M. E. Brezinski, "Evaluation of the adaptive speckle suppression filter for coronary optical coherence tomography imaging," *IEEE Transactions on Medical Imaging*, vol. 19, no. 12, pp. 1261–1266, 2000.

[6] D. C. Adler, T. H. Ko, and J. G. Fujimoto, "Speckle reduction in optical coherence tomography images by use of a spatially adaptive wavelet filter." *Optics Letters*, vol. 29, no. 24, pp. 2878–2880, 2004.

[7] M. R. Avanaki, P. P. Laissue, T. J. Eom, A. G. Podoleanu, and A. Hojjatoleslami, "Speckle reduction using an artificial neural network algorithm," *Applied Optics*, vol. 52, no. 21, pp. 5050–5057, 2013.

[8] Y. Ding and I. W. Selesnick, "Artifact-free wavelet denoising: Non-convex sparse regularization, convex optimization," *IEEE Signal Processing Letters*, vol. 22, no. 9, pp. 1364–1368, 2015.

[9] D. L. Donoho, "De-noising by soft-thresholding," *IEEE Transactions on Information Theory*, vol. 41, no. 3, pp. 613–627, 1995.

[10] S. G. Chang, B. Yu, and M. Vetterli, "Adaptive wavelet thresholding for image denoising and compression," *IEEE Transactions on Image Processing*, vol. 9, no. 9, pp. 1532–1546, 2000.

[11] M. Kaur, K. Sharma, and N. Dhillon, "Image denoising using wavelet thresholding," *International Journal of Engineering and Computer Science*, vol. 2, no. 10, 2013.

[12] S. Boyd, N. Parikh, E. Chu, B. Peleato, J. Eckstein *et al.*, "Distributed optimization and statistical learning via the alternating direction method of multipliers," *Foundations and Trends® in Machine learning*, vol. 3, no. 1, pp. 1–122, 2011.

[13] P. L. Combettes and J. C. Pesquet, "A douglas-rachford splitting approach to nonsmooth convex variational signal recovery," *IEEE Journal of Selected Topics in Signal Processing*, vol. 1, no. 4, pp. 564–574, Dec 2007.

[14] J. Eckstein and D. P. Bertsekas, "On the douglas-rachford splitting method and the proximal point algorithm for maximal monotone operators," *Mathematical Programming*, vol. 55, no. 1-3, pp. 293–318, 1992.

[15] L. Condat, "A direct algorithm for 1-d total variation denoising," *IEEE Signal Processing Letters*, vol. 20, no. 11, pp. 1054–1057, 2013.

[16] I. W. Selesnick and İ. Bayram, "Sparse signal estimation by maximally sparse convex optimization," *IEEE Transactions on Signal Processing*, vol. 62, no. 5, pp. 1078–1092, 2014.

[17] L. Dümbgen and A. Kovac, "Extensions of smoothing via taut strings," *Electronic Journal of Statistics*, vol. 3, pp. 41–75, 2009.

[18] M. K. Garvin, M. D. Abramoff, X. Wu, S. R. Russell, T. L. Burns, and M. Sonka, "Automated 3-d intraretinal layer segmentation of macular spectral-domain optical coherence tomography images," *IEEE Transactions on Medical Imaging*, vol. 28, no. 9, pp. 1436–1447, 2009.

[19] M. D. Abràmoff, M. K. Garvin, and M. Sonka, "Retinal imaging and image analysis," *IEEE Reviews in Biomedical Engineering*, vol. 3, pp. 169–208, 2010.

[20] M. Maggioni, V. Katkovnik, K. Egiazarian, and A. Foi, "Nonlocal transform-domain filter for volumetric data denoising and reconstruction," *IEEE Transactions on Image Processing*, vol. 22, no. 1, pp. 119–133, 2013.